

Spatio-temporal Sequence Prediction with Point Processes and Self-organizing Decision Trees

Oguzhan Karaahmetoglu and Suleyman S. Kozat *Senior Member, IEEE*

Abstract—We investigate spatio-temporal prediction and introduce a novel prediction algorithm. Our approach is based on the point processes, which we use to model the event arrivals in both space and time. Although we specifically use the Hawkes process, other processes can be readily used as provided remarks in the paper. Moreover, we partition the given spatial region into subregions by an adaptive decision tree and model each subregion with individual and interacting point processes. With individual point processes for each subregion, we estimate the time and location of the events using the past event times and locations. Furthermore, thanks to the nonstationary and self-exciting point generation mechanism in the Hawkes process and the adaptive partitioning of the space, we model the data as nonstationary in both time and space. Finally, we provide a gradient based joint optimization algorithm for the adaptive tree parameter and the point process parameters. With the joint optimization, our algorithm can infer the source statistics and adaptive partitioning of the region. We also provide a training algorithm for the online setup, where we update the model parameters with newly arrived points. We provide experimental results on both simulated data and real-life data where we compare our approach with the standard approaches and demonstrate significant performance improvements thanks to the adaptive spatial partitioning mechanism and the joint optimization procedure.

Index Terms—Spatio-temporal Point Process, Earthquake Prediction, Hawkes Process, Adaptive Decision Trees, Nonstationary Time-Series Data, Online Learning.

I. INTRODUCTION

A. Preliminaries

New samples of data are generated and recorded every moment from millions of sensors in different structures. Spatio-temporal data collection is one of the most critical types of the collected data due to its various real-life applications ranging from spatio-temporal prediction and dynamic system modeling to data assimilation [1], [2], [3]. Spatio-temporal data consists of a collection of samples that are ordered by time and distributed along a two-dimensional space. Predicting the time and location of a sample using only the past sample times and locations is spatio-temporal prediction, which carries vital importance due to its applications in real-life problems such as earthquake prediction [2], crime prediction [4], and social action prediction [5]. Precisely estimating the locations

and times of the future earthquake events and criminal activities could save many lives and predicting malfunctions in an electrical grid could reduce the maintenance times and costs [6], [3], [4]. Despite these critical applications, certain difficulties such as the nonstationarity in both time and space in the data restrict the application of standard approaches [7], [8]. Therefore, we introduce a novel prediction algorithm that models point generations in adaptive subregions with interacting point processes.

Many solutions have been introduced due to critical real-life applications. The dominant approach among the solutions seems to be the deep architectures and Recurrent Neural Networks (RNN) in particular [7], [8], [9]. Thanks to the inherent memory of the RNNs, past information can be carried over time to be used in predictions [10]. RNN has different variants that have different state transition mechanisms, which were also applied to the same problem for comparison. Specifically, Long Short Term Memory (LSTM) [11] networks have shown superior performance thanks to their internal gated structure. Convolutional Neural Network (CNN) was also applied to the same problem as it can learn the spatial interactions between different spatial locations [12], [13], [14]. Despite their complex structures and superior learning capabilities, deep architectures assume structured data, i.e. fixed sampling intervals and discretized spatial locations, and not directly applicable to sparse and nonstationary real-life data [7], [15].

Point processes and statistical time-series models are also applied to the same problem as they are more suited to the nonstationary and sparse data [7], [8], [15]. This approach aims to model the spatio-temporal samples directly. Depending on the application, different point processes have been used to model various real-life data such as the Poisson and Hawkes process [16]. Since point processes can only model sample arrival times [17], [18], certain works introduce spatio-temporal point processes where the locations of the samples are also modeled along with the sample times and certain approaches combine deep architectures with point processes as in [7], [8].

Here, we introduce a novel spatiotemporal prediction algorithm. We model the data as nonstationary in both time and space and highly sparse as it is the case in many real-life data [15], [19]. Thus, our approach is based on point processes, where we formulate a point process model for the spatio-temporal prediction problem. We adaptively partition the space into subregions and model the sample observations in each subregion with interacting point processes. In particular, we are using the Hawkes process to model the spatiotemporal data due to its self-exciting property [17]. Other processes

This work is supported in part by Outstanding Researcher Programme Turkish Academy of Sciences.

Suleyman S. Kozat and O. Karaahmetoglu are with the Department of Electrical and Electronics Engineering, Bilkent University, Bilkent, Ankara 06800, Turkey, Tel: +90 (312) 290-2336, Fax: +90 (312) 290-1223, (contact e-mail: {kozat, koguzhan}@ee.bilkent.edu.tr).

Suleyman S. Kozat and O. Karaahmetoglu are also with the Data-Boss A.S., Bilkent Cyberpark, Ankara 06800, (email: {serdar.kozat, oguzhan.karaahmetoglu}@data-boss.com.tr)

can be readily used depending on the application as they are provided remarks in the paper. Thanks to the self-exciting property of the Hawkes process and the adaptive partitioning, we achieve significant performance improvements compared to the standard approaches on real-life problems such as earthquake prediction, where the data is highly sparse and nonstationary [19]. Finally, we provide a gradient based optimization algorithm for our model, where we jointly optimize the partitioning and the point process modeling mechanism. Moreover, our training algorithm is suitable for the online setup where we update the model parameters as new data arrives.

B. Prior Art and Comparisons

Thanks to their superior learning capabilities to model highly nonlinear patterns and complex structures, deep neural networks have been applied to many problems [10], [16], [20]. Certain variants of deep models such as RNNs can model temporal patterns on time-series data thanks to their inherent memory [10]. Although the deep models can model complex nonlinear patterns in data, they are prone to errors under sparse and nonstationary data, which is generally the case in spatio-temporal data [7], [21]. Moreover, the samples in spatio-temporal data are unevenly spaced in time and can be at any arbitrary location, which is not structured as the deep models expect. To circumvent this issue, unstructured data is converted to a structured form by discretizing the time and space axes and binning the samples into fixed-size intervals [16], [22]. However, this conversion changes the problem as the continuous nature of the event times and locations are changed. Furthermore, model estimations will also be generated for the fixed spatio-temporal bins [22]. Unlike this approach, we directly model the continuous data without applying any adhoc preprocessing stage.

Point processes are another approach applied to the spatiotemporal prediction problem [15], [21], [23]. Although the point processes are applicable to time-series data, previous works extend these models for the spatio-temporal prediction [24], [25]. These modifications extend the point processes to model the event locations along with the event times or to independently estimate the locations as in the marked point processes [26]. Finally, certain approaches combine the deep models with the point processes as in [15], [7]. Although this approach benefits from the complex abilities of the deep models capturing the temporal patterns, time and location information are incorporated additively, which is limited to specific applications [27]. Moreover, point process approaches are generally not applicable to online setup as they require the whole training data for the parameter optimization [28]. On the other hand, our model can be used in online setup as the parameters can be updated as new data arrives. We also adaptively partition the spatial region and update the partitioning and the point process models jointly. Therefore, our model captures the time-varying and space-varying characteristics jointly.

We introduce an objective function, which we use to jointly optimize the model parameters. The objective function is

based on the negative log-likelihood, which is widely used for the probabilistic models [15], [21]. Although the standard negative log-likelihood function is used in previous works, we control the behavior of the parameter optimization procedure by introducing additional weights for the terms in the objective function.

C. Contributions

Our main contributions are:

- 1) As the first time in the literature, we present a novel algorithm that adaptively partitions the spatial region into subregions and model the interaction between these subregions jointly, due to the joint gradient based optimization algorithm.
- 2) We introduce a novel spatio-temporal prediction model based on point processes where we optimize the parameters with respect to the likelihood of the model. In addition to the presented training algorithm, we also present a training algorithm for online setups.
- 3) Although our formulation focuses on the self-exciting Hawkes process, our approach is generic so that any other point process can be used depending on the application as provided remarks in the paper.
- 4) We present a formulation for the Hawkes process with adaptive spatial partitioning using decision trees. Thus, our formulation can model space-varying sample observation mechanisms.
- 5) Through an extensive set of experiments on both simulated and real-life data, we show that our model can represent a spatio-temporal data such as earthquake data, which is highly nonstationary and sparse. We compare our approach with the standard well-known methods where we demonstrate significant performance improvements.

D. Organization of the Paper

In the following section, we introduce our problem description. In section III-A, we briefly describe the probabilistic models that we use. In section III-B, we describe the adaptive partitioning of the spatial region and the spatial kernel we have introduced for the standard Hawkes process. In section III-C, we explain the time and location estimation of the samples using our model. In section III-D, we introduce the training procedure for optimizing the model parameters and the objective function of our algorithm. In section IV, we present the experimental results on both simulated and real-life data. Finally, in section V, we give the concluding remarks.

II. MODEL AND PROBLEM DESCRIPTION

We denote the matrices with boldface and uppercase letters, e.g. \mathbf{X} . $\mathbf{X}_{i,j}$ refers to the element of the matrix at the i th row and the j th column. $\mathbf{X}_{i,:}$ is the i th row and $\mathbf{X}_{:,j}$ is the j th column of the matrix \mathbf{X} . We denote the vectors with boldface lowercase letters, e.g. $\mathbf{x} = [x_0, x_1, \dots, x_N]$ is a vector with length N . The notation \mathbf{x}^T refers to the ordinary transpose of a vector and ℓ^2 norm of the vector \mathbf{x} is $\|\mathbf{x}\|^2 = \langle \mathbf{x}, \mathbf{x} \rangle = \mathbf{x}^T \mathbf{x}$.

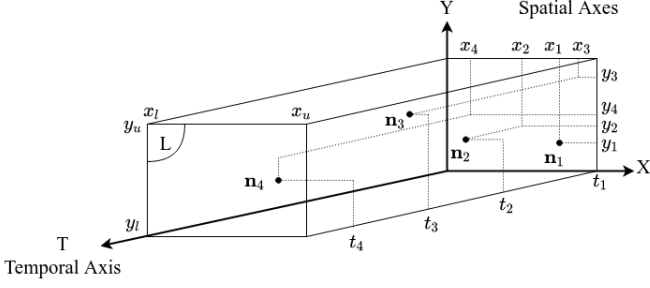


Fig. 1: Illustration of a spatio-temporal sequence with 4 samples, $\{\mathbf{n}_1, \mathbf{n}_2, \mathbf{n}_3, \mathbf{n}_4\}$. Each sample has a location stamp $\{(x_1, y_1), (x_2, y_2), (x_3, y_3), (x_4, y_4)\}$ and a timestamp $\{t_1, t_2, t_3, t_4\}$.

\odot operator is the element-wise multiplication and $\mathbb{1}_N$ is a column vector of ones with length N . All vectors are column vectors and real vectors.

Domain of spatio-temporal data consists of three axes, temporal axis T and spatial axes X and Y as in Fig. 1. Samples $\mathbf{N} = \{\mathbf{n}_i\}_i$ in spatio-temporal data are described by their locations in these three axes with a timestamp and a location stamp $\mathbf{n}_i = [t_i, \mathbf{l}_i]$, where t_i is the position in time, e.g. times of events and $\mathbf{l}_i = (x_i, y_i)$ is a two-tuple describing the spatial position, e.g. latitude and longitude. These positions are visualized in Fig. 1 for 4 samples. Samples are observed in the spatial region L with boundaries $L = [[x_1, x_u], [y_1, y_u]]$ as shown in Fig. 1, i.e. $x_i \in [x_1, x_u]$, $y_i \in [y_1, y_u] \forall \mathbf{n}_i$. We model the data as continuous in both time and space, therefore $t_i \in \mathbb{R}$ and $x, y \in \mathbb{R}$. Moreover, samples are ordered in time, i.e. $t_i > t_j$ for $i > j$. We only use the time and location stamps of the spatio-temporal samples to model the data.

We form the set $\{t_i\}_i$, which consists of the sample observation times. Using the observation times set, we define the "history" $\Omega(t)$ at time t , which is expressed as $\Omega(t) = \{\mathbf{n}_i | t_i < t\}_i$, i.e. observed samples until the time t . Our aim is to predict the observation time and location of a sample $\mathbf{n}_i = [t_i, \mathbf{l}_i]$ using the history $\Omega(t_i)$. Hence, we introduce

$$\hat{\mathbf{n}}_i = [\hat{t}_i, \hat{\mathbf{l}}_i] = F(\Omega(t)), \quad (1)$$

which estimates the time and the location of the sample \mathbf{n}_i , where $\hat{\mathbf{n}}_i = [\hat{t}_i, \hat{\mathbf{l}}_i]$, which are the estimated time and location of the sample \mathbf{n}_i . We assess the performance of our estimation $\hat{\mathbf{n}}_i$ for the sample \mathbf{n}_i with the loss function

$$l(\hat{\mathbf{n}}_i, \mathbf{n}_i) = [(\hat{t}_i - t_i)^2, (\hat{x}_i - x_i)^2 + (\hat{y}_i - y_i)^2]. \quad (2)$$

For I samples, we evaluate the performance with the averaged loss over the samples as

$$L(\hat{N}, N) = \frac{1}{I} \sum_{i=1}^I l(\hat{\mathbf{n}}_i, \mathbf{n}_i), \quad (3)$$

where the sets \hat{N} and N are the estimation and the ground-truth sample pairs.

Remark 1. We can use any ℓ^p loss function instead of using the mean squared error between the estimations and the ground truth values, which are given as

$$l(\hat{\mathbf{x}}_i, \mathbf{x}_i) = [|\hat{t}_i - t_i|^p, |\hat{x}_i - x_i|^p + |\hat{y}_i - y_i|^p]. \quad (4)$$

We compute the predicted time and location of a sample with the function F in (1). We model the sample observation times and locations with a point process model, therefore F is the expected time and location of the sample \mathbf{n}_i , i.e. $(\hat{t}_i, \hat{\mathbf{l}}_i) = \mathbb{E}[\tilde{t}_i, \tilde{\mathbf{l}}_i | \Omega(t_{i-1})]$. Variables \tilde{t}_i and $\tilde{\mathbf{l}}_i$ are random variables, which are the observation time and spatial location of the sample \mathbf{n}_i . Therefore, we give a brief information about the point processes in the next subsection.

A. Representation of Sample Observations with Point Processes

We define the function $N(t)$ as the total number of samples up to time t . For point processes, the density function of the observation time of the sample \mathbf{n}_i is given as

$$f_{\tilde{t}_i}(t | \Omega(t)) = \lim_{\Delta t \rightarrow 0} P(N(t) - N(t - \Delta t) = 1 | \Omega(t)), \quad (5)$$

which is a function of previous samples [18]. We can also express the density function in (5) using the conditional intensity function

$$f_{\tilde{t}_i}(t | \Omega(t)) = \lambda(t | \Omega(t)) e^{-\int_{t_{i-1}}^t \lambda(t' | \Omega(t')) dt'}, \quad (6)$$

if it is approximated by Bernoulli trials as $\Delta t \rightarrow 0$. Point generation mechanisms and the form of the probability density functions of a point process is governed by the choice of the intensity function $\lambda(t | \Omega(t))$ [18]. Definition of the intensity function is given as

$$\lambda(t | \Omega(t)) = \lim_{\Delta t \rightarrow 0} \frac{P(N(t + \Delta t) - N(t) = 1 | \Omega(t))}{\Delta t}, \quad (7)$$

which corresponds to the expected number of observations in an infinitesimal time interval around t .

Different choices of the conditional intensity function will yield different sample generation mechanisms as the magnitude of the intensity control the rate at which the samples are observed. Depending on the formulation, this rate can be constant, time-varying or space-varying [18]. We formulate our algorithm using the Hawkes process intensity, which is a function of the history as

$$\lambda(t | \Omega(t)) = \mu + \sum_{t_j < t} e^{-\gamma(t-t_j)}, \quad (8)$$

where $\{t_j\}_j$ are the times of the sample observations before t , μ is the background intensity and γ is called the decay rate.

Remark 2. Although we give our formulations for the Hawkes process intensity, our approach can be used with other point process intensity formulations. Thus, depending on the application, instead of using the Hawkes process, we could use any other intensity formulation such as the Poisson intensity

$$\lambda(t | \Omega(t)) = \lambda^*, \quad (9)$$

where $\lambda^* \in \mathbb{R}^+$ [17]. We could also use the intensity of the self-correcting process

$$\lambda(t | \Omega(t)) = \mu t - \sum_{t_j < t} \alpha, \quad (10)$$

$\mu, \alpha \in \mathbb{R}^+$ [29].

We choose the Hawkes intensity formulation due to its certain properties. First of all, the dependency on the past samples yields a nonstationary process in time thanks to the temporal kernel $g_i(t-t_j) = e^{-\gamma(t-t_j)}$. Moreover, the effect of the past samples in the intensity is additive and increases with closer sample times. Thus, it is a self-exciting process. This property is useful for modeling certain real-life applications [23], [22]. Nevertheless, spatial location information of the past samples are not incorporated into the formulation. We aim to predict the times and locations of the samples using the observation times and locations of the past samples. To this end, we introduce a conditional intensity function by incorporating the spatial interactions with a spatial kernel mechanism. In the following section, we give details about this spatial kernel.

III. A NOVEL SPATIO-TEMPORAL PREDICTION MODEL BASED ON POINT PROCESSES

We introduce the adaptive spatial partitioning into fixed number of subregions mechanism using decision trees in this section. We give the formulations of the adaptive decision tree structure and then describe the point process optimization procedure in each subregion to represent the sample observations. Finally, we introduce our training procedure and the likelihood-based objective function.

A. Spatio-temporal Conditional Intensity Function with Spatial and Temporal Kernels

Here, we give the formulation for the conditional intensity function that uses a temporal and spatial kernel to model the sample observations with a time and space-varying process. Our spatial kernel is based on decision trees, which forms adaptive spatial partitions and can be updated with the observed samples in an online manner.

Hawkes process intensity is a time-varying function and can change over time based on the past sample observations. However, in spatio-temporal data, the intensity could change in space as well. Thus, the intensity should be expressed as a function of both time and space to model nonstationary real-life data. Consequently, we define the intensity in (7) as the expected number of sample observations in an infinitesimal spatio-temporal interval around the time t and location \mathbf{l} , which is given as

$$\lambda(t, \mathbf{l} | \Omega(t)) = \lim_{\Delta t \rightarrow 0, \Delta l \rightarrow 0} \frac{P(N(t + \Delta t, \bar{\mathbf{l}}) - N(t) = 1 | \Omega(t))}{\Delta t \Delta l} \quad (11)$$

where $\bar{\mathbf{l}}$ is the infinitesimal circular region centered at the location \mathbf{l} with radius Δl , i.e. $\bar{\mathbf{l}} = \{(x, y) \in \mathbb{R}^2 | \|\mathbf{l} - (x, y)\|^2 \leq \Delta l\}$. Consequently, we define $N(t, \bar{\mathbf{l}})$ as the number of events up to time t and the number of events around the spatial location \mathbf{l} at time t .

Since we model the data with a time and space-varying process, we partition the spatial region L into fixed number of subregions, $\{L_k\}_{k=1}^K$. These subregions form a partition of the

whole space, i.e. $\bigcup_{k=1}^K L_k = L$ and $L_i \cap L_j = \emptyset$. We group the samples into subsets depending on their spatial locations, i.e. $\mathbf{N}_k = \{\mathbf{n}_i | \mathbf{l}_i \in L_k\}_i$, which also partition the samples. We also define the vector $\boldsymbol{\rho}(\mathbf{l}) = [\rho_k(\mathbf{l})]_{k=1}^K \forall \mathbf{l} \in L$, which is the subregion vector where

$$\rho_k(\mathbf{l}) = \begin{cases} 1, & \text{if } \mathbf{l} \in L_k \\ 0, & \text{otherwise.} \end{cases} \quad (12)$$

One-hot vector $\boldsymbol{\rho}(\mathbf{l})$ indicates the subregion containing the location \mathbf{l} . For each subregion, we represent the sample observations with an individual point process model, hence with an individual conditional intensity. For the subregion L_k , the conditional intensity is $\lambda_k(t, \Omega(t))$. As a result, we express the conditional intensity for any arbitrary location as $\lambda(t, \mathbf{l} | \Omega(t))$, which is the conditional intensity of the subregion L_k . It is given as,

$$\lambda(t, \mathbf{l} | \Omega(t)) = \begin{cases} \lambda_1(t | \Omega(t)), & \text{if } \mathbf{l} \in L_1 \\ \lambda_2(t | \Omega(t)), & \text{if } \mathbf{l} \in L_2 \\ \dots & \\ \lambda_K(t | \Omega(t)), & \text{if } \mathbf{l} \in L_K. \end{cases} \quad (13)$$

As an alternative, we can express the conditional intensity as

$$\lambda(t, \mathbf{l} | \Omega(t)) = \boldsymbol{\rho}(\mathbf{l})^T \boldsymbol{\lambda}(t, \mathbf{l} | \Omega(t)), \quad (14)$$

where $\boldsymbol{\lambda}(t, \mathbf{l} | \Omega(t)) = [\lambda_k(t, \mathbf{l} | \Omega(t))]_{k=1}^K$.

In order to incorporate the location information of the past samples, we also add a spatial kernel to the intensity $\lambda_k(t | \Omega(t))$ as

$$\lambda_k(t | \Omega(t)) = \mu_k + \sum_{t_j < t} g_{t,k}(t - t_j) g_{l,k}(\mathbf{l}_j), \quad (15)$$

where the temporal kernel $g_{t,k}(t - t_j)$ is selected as in (8) due to the self-exciting property. We formulate the spatial kernel $g_{l,k}(\mathbf{l}_j)$ in (15) as

$$g_{l,k}(\mathbf{l}_j) = \boldsymbol{\Gamma}_{:,k}^T \boldsymbol{\rho}(\mathbf{l}_j), \quad (16)$$

where $\boldsymbol{\Gamma}$ is a $K \times K$ matrix modeling the interaction among the samples in all subregions, which is referred to as the interaction matrix. The element $\boldsymbol{\Gamma}_{k,l}$ corresponds to the effect of a sample $\mathbf{n} \in \mathbf{N}_k$ in the subregion L_k to the intensity of the l th subregion.

Note that the summation in (15) accumulates the effects of all the past samples. In online setup, this summation would grow indefinitely, however, the exponential kernel in the temporal kernel allows us to truncate the summation with the ν most recent elements. To this end, we ignore the rest of the samples and define the set $\mathbf{N}_\Omega(t, \nu)$, which contains the most recent ν samples before time t .

We form spatial subregions using decision trees that are adaptively organized in time. Thus, as the intensity functions are organized with new samples, boundaries of the spatial subregions are also organized. In the following section, we give details about the adaptive tree structure.

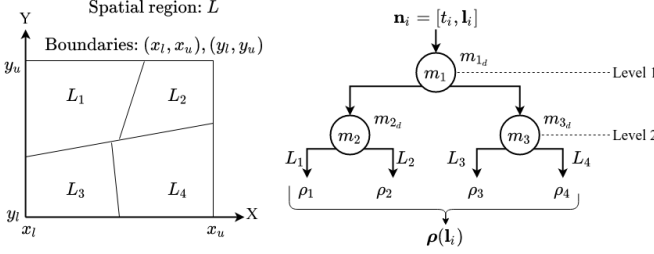


Fig. 2: Diagram of a 2-level tree, which has three nodes m_1 , m_2 , m_3 . At every node, a decision function is computed, which are shown as m_{1d} , m_{2d} , m_{3d} . Subregion scores $\rho(\mathbf{l}_i)$ are computed for 4 branch leaves for the input samples $\mathbf{n}_i = [t_i, \mathbf{l}_i]$. Each leaf node is associated with a spatial subregion, which are L_1 , L_2 , L_3 and L_4 for the 4 branches.

B. Adaptive Partitioning of the Spatial Region with Decision Trees

The decision tree in our algorithm consists of a collection of nodes $D = \{m_r\}_{r=1}^R$ that are placed hierarchically as in Fig. 2. Each node, except the leaf nodes (located at the bottom of the tree, at level $\ell = 2$), has two children that are linked with branches. The top node, m_1 , is referred to as the root node.

Remark 3. Note that in Fig. 2 we illustrate a 2-level tree for simplicity. Our formulation covers different depths as well.

The sample \mathbf{n}_i is assigned to a spatial subregion using the decision tree. At each node, the sample is either assigned to left or right node starting from the root node until reaching to a leaf node. A decision function, m_{rd} with range $\{-1, +1\}$, is computed at each node, which uses the features of the input sample. In certain works, a randomly selected feature from the input sample is used at each node for comparison [30], [31], where the input has features $\mathbf{n}_i = [n_i^{(f)}]_{f=1}^F$. The decision function is given as

$$m_{rd}(\mathbf{n}_i) = \text{sign}(n_i^{(m_{ri})} - m_{rb}) \leq 0, \quad (17)$$

where $n_i^{(m_{ri})}$ is the feature used at the node m_r and m_{rb} is the threshold for comparison. The sample \mathbf{n}_i is assigned to the left node if (17) is positive and to the right node otherwise.

Samples are separated by their features with the decision functions as in (17). In our case, features of the samples are only the location vector $\mathbf{l} = (x_i, y_i)$. Therefore, we separate the samples by comparing their spatial components with threshold values. As the depth of the tree grows, the number of spatial subregions will also increase. For a depth- ℓ decision tree, we have $K = 2^\ell$ leaf branches for the subregions $\{L_k\}_{k=1}^K$ as in Fig. 2.

Instead of using a single feature for comparison as in (17), we use all features $[n_i^{(f)}]_{f=1}^F$ for comparison. Hence, the decisions have the form

$$m_{rd}(\mathbf{n}_i) = \text{sign}(m_{rw}^T \mathbf{l}_i - m_{rb}) \leq 0, \quad (18)$$

where m_{rw} is the weight vector combining the location elements x_i , y_i . With such decision functions, we partition the space with lines as in Fig. 2.

Remark 4. We use a decision tree to separate the feature

space, which results in linear decision boundaries. We could use any nonlinear function of the spatial coordinates, e.g.

$$f(x_i, y_i) = g(\mathbf{w}_x x_i + \mathbf{w}_y y_i + b), \quad (19)$$

where $\{\mathbf{w}_x, \mathbf{w}_y\}$ are $K \times 1$ weight vectors and g is a nonlinear function. We can generate the vector $\rho(x_i, y_i)$ by setting the maximum element of $f(x_i, y_i)$ to 1 and the rest to 0, which generates a one-hot vector as in the decision tree partitioning. However, this formulation for the spatial separation could result in an unnecessary and complex partitioning [32].

We adapt the boundaries of the spatial region by updating the weight parameters in (12). Instead of using hard functions in the decision functions, we use the sigmoid function ($\sigma(x) = 1/(1 + e^{-x})$) as

$$m_{rd}(\mathbf{n}_i) = \sigma(m_{rw}^T \mathbf{n}_i - m_{rb}), \quad (20)$$

which yields a score in $[0, 1]$. Soft functions in decision functions as in (20) were previously used in [33] for source coding. In the standard formulation given in (18), a sample is either assigned to the left branch or to the right branch. As a result, a sample can only lie in a single subregion, which was expressed with a one-hot vector as in (12). However, by using a soft function in the decision function, this hard separation is removed. In this case, the sample \mathbf{n}_i is assigned to both the left branch and to the right branch with scores $m_{rd}(\mathbf{n}_i)$ and $1 - m_{rd}(\mathbf{n}_i)$.

In the standard formulation with hard decision functions, we represent the spatial subregion score vector with a one-hot vector. However, in this case, the subregion score vector is $\rho(\mathbf{l}_i) = [\rho_k(\mathbf{l}_i)]_{k=1}^K$ where $\rho_k(\mathbf{l}_i) \in [0, 1] \forall k$. We compute the scores by multiplying the scores obtained at each layer starting from the root node until the leaf branches as

$$\rho_k(\mathbf{n}_i) = \prod_{l=1}^{\ell} \pi(\mathbf{n}_i, \nu_k^{(l)}, \tau_k^{(l)}), \quad (21)$$

where

$$\pi(\mathbf{n}_i, \nu_k^{(l)}, \tau_k^{(l)}) = \begin{cases} \nu_k^{(l)}(\mathbf{n}_i), & \tau_k^{(l)} = \text{left} \\ 1 - \nu_k^{(l)}(\mathbf{n}_i), & \tau_k^{(l)} = \text{right}. \end{cases} \quad (22)$$

We define the sequence of branches and sequence of visited nodes to reach the k th leaf as τ_k and ν_k , e.g. for the depth-2 tree shown in Fig. 2, second leaf branch ρ_2 is reached by taking first the left branch and then the right branch. Thus, $\tau_2 = [\text{left}, \text{right}]$ and $\nu_2 = [m_1, m_2]$. $\nu_k^{(l)}$ in (21) and (22) is the visited node at level l to reach the k th leaf. $\tau_k^{(l)}$ is the direction of the branch at level l to reach the k th leaf. The decision function score at level l is expressed as $\pi(\mathbf{n}_i, \nu_k^{(l)}, \tau_k^{(l)})$.

Remark 5. The following properties are satisfied by the subregion score vector:

- The maximum subregion score is obtained for the subregion containing the spatial location, \mathbf{l}_i of the sample \mathbf{n}_i , i.e. $\kappa = \arg \max_{k \in \{0, 1, \dots, K\}} [\rho_k(\mathbf{n}_i)] \Leftrightarrow \mathbf{l}_i \in L_\kappa$.
- Subregion scores sum up to 1 for any location $\mathbf{l}_i \in L$, i.e. $\sum_{k=1}^K \rho_k(\mathbf{l}_i) = 1$.

The spatial subregion vector of scores $\rho(\mathbf{n}_i)$ are computed by an adaptive decision tree, which is used in the spatial kernel mechanism in (16). In the next section, we explain the estimation of the sample times and locations using the spatio-temporal density function. Moreover, we also explain the procedure for optimizing the model parameters given data.

C. Sample Time and Location Prediction

In order to estimate the time and location of samples, we formulate the joint density function $f_{\tilde{t}_i, \tilde{\mathbf{l}}_i}$, using the intensity (11) and the density in (6). The joint density function is

$$f_{\tilde{t}_i, \tilde{\mathbf{l}}_i}(t, \mathbf{l} | \Omega(t_{i-1})) = \lambda(t, \mathbf{l} | \Omega(t_{i-1})) e^{-\Lambda_{t_{i-1}}(t, \mathbf{l})}, \quad (23)$$

$$\Lambda_{t_{i-1}}(t, \mathbf{l}) = \int_{t_{i-1}}^t \int_L \lambda(t', \mathbf{l}' | \Omega(t_{i-1})) d\mathbf{l}' dt'.$$

We use a more compact expression for the conditional intensity as in (14), which corresponds to the weighted average of the subregion intensities $\lambda(t, \mathbf{l} | \Omega(t_{i-1}))$. Therefore,

$$\lambda(t, \mathbf{l} | \Omega(t_{i-1})) = \rho(\mathbf{l})^T \lambda(t, \mathbf{l} | \Omega(t_{i-1})). \quad (24)$$

Note that in (24), the computations include an integration. We estimate the integration with the Riemann sum [34]. Thus, uniformly spaced samples $\{\mathbf{n}_j\}_j$ in time and space are sampled for the computation. For example, the exponent $\Lambda_{t_{i-1}}(t, \mathbf{l})$ is calculated as

$$\Lambda_{t_{i-1}}(t, \mathbf{l}) = \frac{1}{M} \sum_{t_j, \mathbf{l}_j} \lambda(t_j, \mathbf{l}_j | \Omega(t_{i-1})) |T| |L|, \quad (25)$$

where M is the number of points used in the integration estimation. In our experiments, we have observed that choosing a sufficiently large number of points does not cause any negative effects on the performance. We sample the points \mathbf{n}_j at times t_j and at locations \mathbf{l}_j . Finally, the terms $|T|$ and $|L|$ are the length and area of the temporal and spatial boundaries of the integration respectively. We compute $|T| = t - t_{i-1}$ and $|L| = (x_u - x_l) \times (y_u - y_l)$.

Remark 6. *Instead of using the Riemann sum for the integrations, we could use the Monte Carlo Integration method [35], which is preferred over Riemann sum when the function has abrupt changes. To circumvent this issue, we can readily increase the number of sampled points in the Riemann sum given in (25). In our experiments, we have observed that choosing a sufficiently large number of samples does not have a negative effect on the performance.*

To estimate the sample time and location, we marginalize the joint density function over time and space to obtain the marginal density functions as

$$f_{\tilde{t}_i}(t) = \int_L f_{\tilde{t}_i, \tilde{\mathbf{l}}_i}(t, \mathbf{l} | \Omega(t_{i-1})) d\mathbf{l}, \quad (26)$$

$$f_{\tilde{\mathbf{l}}_i}(\mathbf{l}) = \int_{t_{i-1}}^\infty f_{\tilde{t}_i, \tilde{\mathbf{l}}_i}(t, \mathbf{l} | \Omega(t_{i-1})) dt.$$

We compute the estimated time and location of the sample \mathbf{n}_i as the conditional mean of the random variables \tilde{t}_i and $\tilde{\mathbf{l}}_i$ as

$$\hat{t}_i = \mathbb{E}[\tilde{t}_i | \Omega(t_{i-1})] = \int_{t_{i-1}}^\infty t' f_{\tilde{t}_i}(t' | \Omega(t_{i-1})) dt', \quad (27)$$

$$\hat{x}_i = \mathbb{E}[\tilde{x}_i | \Omega(t_{i-1})] = \int_L x' f_{\tilde{\mathbf{l}}_i}(x' | \Omega(t_{i-1})) d\mathbf{l}, \quad (28)$$

$$\hat{y}_i = \mathbb{E}[\tilde{y}_i | \Omega(t_{i-1})] = \int_L y' f_{\tilde{\mathbf{l}}_i}(y' | \Omega(t_{i-1})) d\mathbf{l}, \quad (29)$$

where the integration in (28) and (29) is over the region L .

The integration computations in (26) and (27) are over an infinitely long time interval. Thus, computing the estimations numerically would not be possible. However, the conditional intensity function in (7) is by definition, a non-negative function. The density function in (23) is therefore a monotonically decreasing function of time. Hence, we compute the Riemann sum of the integration up to a certain time. We select this time as $20 \times \Delta t$, where Δt is the mean inter-arrival time between samples, i.e. $\Delta t = (t_I - t_1)/I$. We observe that this selection is sufficient for our experiments.

The integration computation in (23) is between the time of the last event and any time t . Computing this integration for two arbitrary times $t' > t'' > t_{i-1}$ from scratch would be unnecessary as they share a common interval. Therefore, we sort the sampled points in the Monte Carlo or Riemann sum estimation in (25). Starting from the closest point in time, we accumulate the intensity towards the furthest point and keep the accumulated intensity in memory.

D. Model Parameter Optimization via Likelihood Maximization

Here, we describe the objective function that we are using to update the model parameters and the gradient based optimization procedure.

Parameters of the node m_r are the weights $m_{r\mathbf{w}}$ applied on the samples features and the threshold m_{rb} used for comparison. For the decision tree, model parameters are the collection of node parameters $\Theta_{\text{tree}} = \{(m_{r\mathbf{w}}, m_{rb})\}_{r=1}^R$ for R nodes. We can also group the point process parameters for K subregions. For a single subregion, the intensity in (15) has the parameters μ_k and γ_k . Interaction matrix Γ is a common parameter for all subregions. All parameters for all subregions are $\Theta_{\text{hawkes}} = \{\Gamma, \{(\mu_k, \gamma_k)\}_{k=1}^K\}$.

Combining the two sets, we form the set of model parameters $\Theta = [\Theta_{\text{tree}}, \Theta_{\text{hawkes}}]$. Full notation for the density function $f_{\tilde{t}_i, \tilde{\mathbf{l}}_i}(t, \mathbf{l} | \Omega(t_i))$ and $\lambda(t_j, \mathbf{l}_j | \Omega(t_j))$ are $f_{\tilde{t}_i, \tilde{\mathbf{l}}_i}(t, \mathbf{l} | \Omega(t_i), \Theta)$ and $\lambda(t_j, \mathbf{l}_j | \Omega(t_j), \Theta)$ respectively. We drop the term Θ from the notation for simplicity.

We compute the likelihood of our model using

$$\mathcal{L}(\mathbf{N}) = \prod_{i=1}^I f_{\tilde{t}_i, \tilde{\mathbf{l}}_i}(t_i, \mathbf{l}_i | \Omega(t_{i-1})). \quad (30)$$

We find the optimal set of model parameters Θ^* by randomly initializing a set of model parameters Θ_0 and updating the set with the stochastic gradient-ascent algorithm [36]. To remove the exponential terms in (30), we compute the gradients with respect to the log-likelihood $\tilde{\mathcal{L}} = \log \mathcal{L}$, which is

$$\tilde{\mathcal{L}}(\mathbf{N}) = \sum_{i=1}^I \log f_{\tilde{t}_i, \tilde{\mathbf{l}}_i}(t_i, \mathbf{l}_i | \Omega(t_{i-1})). \quad (31)$$

Using the definition of $f_{\tilde{t}_i, \tilde{\mathbf{l}}_i}(t_i, \mathbf{l}_i | \Omega(t_{i-1}))$ in (31) with the formulation in (23), we obtain

$$\tilde{\mathcal{L}}(\mathbf{N}) = \sum_{i=1}^I \log \lambda(t_i, \mathbf{l}_i | \Omega(t_{i-1})) - \sum_{j=1}^J \Lambda_{t_{i-1}}(t_j, \mathbf{l}_j), \quad (32)$$

which has two terms, $\mathcal{L}_{\text{positive}}$ and $\mathcal{L}_{\text{negative}}$. The integration in $\mathcal{L}_{\text{negative}}$ can be accumulated in time and expressed as a single integration as

$$\mathcal{L}_{\text{negative}} = \int_{t_0}^T \int_L \lambda(t', \mathbf{l}' | \Omega(t_{i-1})) d\mathbf{l}' dt', \quad (33)$$

where t_0 is the start of the integration simulation and T is the end time. We sample uniformly spaced points in both time and space for the integration in (33) as in [15]. $\mathcal{L}_{\text{positive}}$ accumulates the log-intensities of the sample observations and $\mathcal{L}_{\text{negative}}$ penalizes the intensity function for the sampled points, which represent the rest of the spatio-temporal interval. We sum the two terms with a weight term as

$$\tilde{\mathcal{L}} = \mathcal{L}_{\text{positive}} + \alpha \mathcal{L}_{\text{negative}}, \quad (34)$$

to control the effect of the negative and the positive terms on the overall $\tilde{\mathcal{L}}$.

We define the optimal parameters as the set of model parameters Θ^* that exceeds a certain tolerance level for the log-likelihood \mathcal{L}_{tol} , i.e.

$$\mathcal{L}(\mathbf{N} | \Theta^*) \geq \mathcal{L}_{\text{tol}} \quad (35)$$

To compute the optimal set of parameters, we split the given set of samples $\mathbf{N} = \{\mathbf{n}_i\}_{i=1}^I$ into three subgroups; training set ($\mathbf{N}_{\text{train}} = \{\mathbf{n}_i\}_{i=1}^{I_{\text{train}}}$), validation set ($\mathbf{N}_{\text{val}} = \{\mathbf{n}_i\}_{i=I_{\text{train}}+1}^{I_{\text{val}}}$) and test set ($\mathbf{N}_{\text{test}} = \{\mathbf{n}_i\}_{i=I_{\text{val}}+1}^I$). We use the training set for the parameter optimization. We measure the performance of the parameters using the validation and the test sets with the metric in (3).

We update the set of parameters starting from the initial values Θ_0 with the gradient updates. For a model parameter $\theta \in \Theta$ we have

$$\theta_{i+1} = \theta_i + \eta \nabla_{\theta} \tilde{\mathcal{L}}(\mathbf{N}_B), \quad (36)$$

where \mathbf{N}_B is a mini-batch consisting of randomly picked samples from the training set $\mathbf{N}_{\text{train}}$. The learning rate η scales the magnitudes of parameter updates and $\nabla_{\theta} \tilde{\mathcal{L}}(\mathbf{N}_B)$ is the gradient vector of $\tilde{\mathcal{L}}(\mathbf{N}_B)$ with respect to the parameter θ . Using (32) and (34), we have

$$\frac{\partial \tilde{\mathcal{L}}(\mathbf{N}_B)}{\partial \theta} = \frac{1}{B} \sum_{b=1}^B \left(\left[\frac{1}{\lambda_k(t_b, \mathbf{l}_b)} \right]_{k=1}^K + \alpha \mathbb{1}_K \right) \odot \frac{\partial \lambda(t_b, \mathbf{l}_b)}{\partial \theta}. \quad (37)$$

Partial derivatives of λ with respect to the Hawkes parameters are

$$\frac{\partial \lambda_k(t_b, \mathbf{l}_b)}{\partial \gamma_k} = \mathbf{\Gamma}_{:,k}^T \sum_{\mathbf{n} \in \mathbf{N}_{\Omega(t_b, \nu)}} \rho_k(\mathbf{l})(t - t_b) e^{\gamma_k(t - t_b)}, \quad (38)$$

$$\frac{\partial \lambda_k(t_b, \mathbf{l}_b)}{\partial \mathbf{\Gamma}_{i,k}} = \sum_{\mathbf{n} \in \mathbf{N}(t_b, \nu)} \rho_i(\mathbf{l}) e^{\gamma_k(t - t_b)} \quad (39)$$

and

$$\frac{\partial \lambda_k(t_b, \mathbf{l}_b)}{\partial \mu_k} = \rho_k(\mathbf{l}_b). \quad (40)$$

Similarly, the derivatives of the tree parameters are

$$\frac{\partial \lambda_k(t_b, \mathbf{l}_b)}{\partial \rho} = \lambda(t_b, \mathbf{l}_b) \odot (\mathbb{1}_K + \mathbf{J}^T \mathbf{p}(\mathbf{l}_b)), \quad (41)$$

where \mathbf{J} is the jacobian matrix. The element $\mathbf{J}_{i,j}$ corresponds to $\partial \lambda_i / \partial \rho_j$. Derivative of the weight vector $m_{r\mathbf{w}}$ is

$$\frac{\partial \rho(\mathbf{l}_b)}{\partial m_{r\mathbf{w}}} = \sum_{k=1}^K \prod_{\substack{l=1, \\ l \neq l'}}^L \pi(\mathbf{n}_b, \nu_k^{(l)}, \tau_k^{(l)}) \sigma(1 - \sigma) \mathbf{l}_b. \quad (42)$$

where l' is the level of the node m_r . Similarly,

$$\frac{\partial \rho(\mathbf{l}_b)}{\partial m_{r\mathbf{b}}} = \sum_{k=1}^K \prod_{\substack{l=1, \\ l \neq l'}}^L \pi(\mathbf{n}_b, \nu_k^{(l)}, \tau_k^{(l)}) \sigma(1 - \sigma), \quad (43)$$

where $\sigma = \sigma(m_{r\mathbf{w}}^T \mathbf{l}_b + m_{r\mathbf{b}})$.

Due to its definition in (11), the conditional intensity should be a non-negative function. Optimizing the model parameters with gradient based updates without imposing any constraint would result in a negative intensity. Thus, we use the softplus function

$$\tilde{\lambda}(t, \mathbf{l} | \Omega(t)) = \log(1 + e^{\lambda(t, \mathbf{l} | \Omega(t))}) \quad (44)$$

to make the intensity non-negative through optimization steps.

The parameters that are not included in the set Θ are the hyperparameters. It consists of the parameters that are not optimized during the training procedure. These parameters are: α , the log-likelihood weighting parameter; \mathcal{L}_{tol} , the tolerance level for the log-likelihood; η , the learning rate that scales the parameter updates; ν , the number of past samples in the intensity computation in (7); J , the number of samples for integration simulations in (27), (33); ℓ , the decision tree depth.

Our optimization algorithm is presented in Algorithm 1, which is an iterative optimization procedure. We first randomly initialize a decision tree with depth ℓ and point processes corresponding to all subregions. At the iteration i , we first compare the current log-likelihood with the tolerance level \mathcal{L}_{tol} . If it is not exceeded, we compute the positive log-likelihood of the model with the current parameters. We also sample points in the spatio-temporal interval and compute the negative term in the log-likelihood using these points. Using the log-likelihood, we compute the parameter updates, $\Delta \theta_i$ for each model parameter. If the tolerance level is achieved at a step, we terminate the training process.

To find the best set of hyperparameters, we perform multiple training runs with a different set of hyperparameters. At the end of each training, we compute the validation performance

Algorithm 1 Likelihood based first-order gradient training procedure.

Require: Hyperparameters, Samples N

$i = 0$

Randomly initialize parameters, $\theta_{\text{tree}}, \theta_{\text{hawkes}}$.

$\Theta_i = [\theta_{\text{tree}}, \theta_{\text{hawkes}}]$

Sample J negative points $\{[t_j, x_j, y_j]\}_{j=1}^J$

$\tilde{\mathcal{L}}_{\text{positive}} \leftarrow \sum_{i=1}^I \log \lambda(t_i, \mathbf{l}_i | \Omega(t_{i-1}))$

$\tilde{\mathcal{L}}_{\text{negative}} \leftarrow \sum_{j=1}^J \Lambda_{t_j}(t_j, \mathbf{l}_j)$

$\tilde{\mathcal{L}} \leftarrow \tilde{\mathcal{L}}_{\text{positive}} + \alpha \tilde{\mathcal{L}}_{\text{negative}}$

while $\tilde{\mathcal{L}} < \log \mathcal{L}_{\text{tol}}$ **do**

Sample J negative points $\mathbf{J} \leftarrow \{[t_j, x_j, y_j]\}_{j=1}^J$

$\tilde{\mathcal{L}}_{\text{positive}} \leftarrow \sum_{i=1}^I \log \lambda(t_i, \mathbf{l}_i | \Omega(t_{i-1}))$

$\tilde{\mathcal{L}}_{\text{negative}} \leftarrow \sum_{j=1}^J \Lambda_{t_j}(t_j, \mathbf{l}_j)$

$\tilde{\mathcal{L}} \leftarrow \tilde{\mathcal{L}}_{\text{positive}} + \alpha \tilde{\mathcal{L}}_{\text{negative}}$

Compute updates, $\Delta \theta_i \leftarrow \nabla_{\theta} \tilde{\mathcal{L}}(\mathbf{N}, \mathbf{J})$

$\theta_{i+1} \leftarrow \theta_i + \eta * \Delta \theta_i$

$i \leftarrow i + 1$

end while

using the metric in (3) on the validation set. We pick the set that yields the least error in estimations. After the best set of hyperparameters are found, we compute the test performance with the same metric and report it.

Although the procedure presented in Algorithm 1 uses the whole set of samples for the optimization, we also present an online training procedure in Algorithm 2. In this procedure, parameters are updated as new samples are observed.

Directly using the log-likelihood formulation given in (31) is not suitable for the online setup as it accumulates the intensity values for all past samples. Thus, we define another log-likelihood function particularly for the online setup, which only samples points after the last event time as

$$\mathcal{L}_{\text{nonline}} = - \sum_{j=1}^J \lambda(t_j, \mathbf{l}_j | \Omega(t_{i-1})), \quad (45)$$

where the sampled points $\{\mathbf{n}_j\}_j$ are in the interval $[t_{i-1}, t_{i-1} + \delta_{i-1}]$ where δ_{i-1} is the temporal length. We choose this length as $20 \times \Delta t$, which yielded an adequate performance in our experiments. Similarly, we modify the term $\mathcal{L}_{\text{positive}}$ as

$$\mathcal{L}_{\text{ponline}} = \log \lambda(t_i, \mathbf{l}_i | \Omega(t_{i-1})). \quad (46)$$

In the online procedure, we only keep the most recent ν samples in the set \mathbf{N} as other samples will not be used any computation. Therefore, in Algorithm 2, we can infer the spatial subregion boundaries and the point process parameters jointly and in an online manner without any growing memory issue.

Remark 7. In our training procedures, we use the stochastic gradient-ascent method, which uses the first order derivatives to update the model parameters with respect to an objective function. To increase the convergence speed of our training procedures, we also use the ADAM optimizer [37], which uses the first order derivatives. Thus, it does not introduce

Algorithm 2 Online training procedure.

Require: Hyperparameters

Randomly initialize parameters, $\theta_{\text{tree}}, \theta_{\text{hawkes}}$.

$\mathbf{N} \leftarrow \{\}$

$\theta \leftarrow [\theta_{\text{tree}}, \theta_{\text{hawkes}}]$

while \mathbf{n} arrives **do**

Sample J negative points $\mathbf{J} \leftarrow \{[t_j, x_j, y_j]\}_{j=1}^J$

$\mathbf{N} \leftarrow \{\mathbf{N}_{\nu-1}, \mathbf{n}\}$

$\mathcal{L}_{\text{ponline}} \leftarrow \log \lambda(t_i, \mathbf{l}_i | \Omega(t_{i-1}))$

$\mathcal{L}_{\text{nonline}} = - \sum_{j=1}^J \lambda(t_j, \mathbf{l}_j | \Omega(t_{i-1}))$

Compute updates, $\Delta \theta \leftarrow \nabla_{\theta} \tilde{\mathcal{L}}(\mathbf{N}, \mathbf{J})$

$\theta \leftarrow \theta + \eta * \Delta \theta$

end while

Models	L	ν	α	N
Experiment-1	2	20	1000	5000
Experiment-2	4	20	1000	5000
Experiment-3	5	20	500	6000
Experiment-4	6	20	500	6000
TreeHawkes	5	20	2000	5000

TABLE I: Hyperparameters used in the simulated data (Experiment-1, Experiment-2, Experiment-3, Experiment-4) and the real-life data experiments (TreeHawkes).

any computational cost for the update equations.

IV. SIMULATIONS AND EXPERIMENTS

In this section, we demonstrate the performance of our algorithm on simulated and real-life data. On real-life data, we compare the performance of our approach with the baseline models. Our experiments are grouped under two categories. In the first category, we simulate an artificial spatio-temporal sequence using our model structure. In the second category, we use a real-life earthquake data to predict the sample times and locations of the events.

Mean squared error in the time estimations in (4) are referred to as $\text{MSE} - t$ and the mean squared error in the location estimations are $\text{MSE} - l$. We refer to our model as "TreeHawkes" in the figures and tables.

A. Experiments on the Simulated Data

We artificially created a set of spatio-temporal sequences, which are generated by our point process model. We have generated different sequences with different hyperparameters to test our model under different setups. We generate the samples using the thinning algorithm [38]. We have tested our model with four experiments on the simulated data.

We construct the models with the hyperparameters given in Table I, which are labeled as "Experiment-1", "Experiment-2", "Experiment-3" and "Experiment-4" for four experiments. For all these experiments, we generate 20 sequences consisting of 5000 samples each, where the model parameters for different experiments are selected randomly. Then, we randomly initialize our model using the same hyperparameters and optimize its parameters using the procedure presented in Algorithm 1 on the training section of the whole sequence. Length of the training, validation and the test set are selected as 3000, 1000

Models	MSE - t	MSE - l
Experiment-1	0.072	9.34
Experiment-2	0.081	8.71
Experiment-3	0.077	7.52
Experiment-4	0.116	6.58
TreeHawkes	0.162	6.47
Linear	0.271	33.28
RNN	0.202	31.86
CNN	0.264	25.47
RSTPP	0.192	15.6
RMTPP	0.189	19.2

TABLE II: Test error scores achieved on simulated data (Experiment-1, Experiment-2, Experiment-3, Experiment-4) and by the TreeHawkes on real-life data, and the baseline models on real-life data.

and 1000 respectively. Moreover, we generate the samples inside the spatial region $L = \{(x, y) \in \mathbb{R}^2 \mid -10 < x < 10, -10 < y < 10\}$. We plot the $MSE - t$ and $MSE - l$ on the validation set in Fig. 3. Finally, the test score for all four experiments are given in Table II.

As it can be seen from Fig. 3 and Table II, we can conclude that as the depth of the tree gets larger, model converges slower to a certain level. Moreover, we can see that the deeper models yield less spatial prediction errors whereas more temporal prediction errors. Less error in the location predictions is due to the modeling of the spatio-temporal sequences in smaller subregions. However, generating more subregions also increase the time required to converge to a certain level as the number of parameters grow exponentially with each new layer.

B. Experiments on Real-life Earthquake Data

To test our model on a real-life dataset, we have used the Significant Earthquakes Dataset [39] as it fits to our problem description. The dataset is recorded by the National Earthquake Information Center (NEIC). The dataset contains entries of earthquake event records associated with their latitude, longitude, depth, magnitude and date and it covers all the earthquake events from 1900 to 2000 that have a magnitude higher than 5.5. Location and time prediction of the earthquake events using the past data fits to our problem since the events are spatio-temporal samples.

Since the dataset only contains the earthquake event records with magnitudes higher than 5.5, it excludes the aftershock records. Aftershocks of earthquakes could have been effectively modeled by the Hawkes process formulation [19]. To this end, we choose a particular spatial region L between the latitudes 31.92° and 72.05° and between the longitudes 110.2° and 180.1° from the whole data, which contains a large number of sequential earthquakes. This region corresponds to the east of China and Russia and all of Japan and Korea.

We convert the earthquake records to spatio-temporal sequence $\mathbf{N} = \{\mathbf{n}_i\}_{i=1}^I$. In particular, we generate 20 sequences by splitting the data into equal-length parts in time, i.e. 5 years. We further process the data by converting the dates of the events to time differences with respect to the first event time in seconds and scale the differences as $\{t_i / (3600 \times 24 \times 30)\}_{i=1}^I$. Moreover, the spatial locations, i.e. latitude and longitude of

the events are scaled as $L = \{(x, y) \in \mathbb{R}^2 \mid -10 < x < 10, -10 < y < 10\}$.

We compute the performance on the real-life data and compare our performance with certain approaches. First model in our comparison is the linear regression (we refer to as Linear), which predicts the displacement in time and space using the past displacement vectors with a linear model. Predictions are computed as

$$\begin{aligned}\Delta t_i &= \mathbf{w}_{tt}^T [\Delta t_{i-k}]_{k=1}^K + \mathbf{w}_{tx}^T [\Delta x_{i-k}]_{k=1}^K + \mathbf{w}_{ty}^T [\Delta y_{i-k}]_{k=1}^K, \\ \Delta x_i &= \mathbf{w}_{xt}^T [\Delta t_{i-k}]_{k=1}^K + \mathbf{w}_{xx}^T [\Delta x_{i-k}]_{k=1}^K + \mathbf{w}_{xy}^T [\Delta y_{i-k}]_{k=1}^K, \\ \Delta y_i &= \mathbf{w}_{yt}^T [\Delta t_{i-k}]_{k=1}^K + \mathbf{w}_{yx}^T [\Delta x_{i-k}]_{k=1}^K + \mathbf{w}_{yy}^T [\Delta y_{i-k}]_{k=1}^K,\end{aligned}\quad (47)$$

which are using the K most recent observations. As the number increases, capability of this model increases, however, we tune this number using the validation performance so that the generalization performance does not decrease [40]. As it can be seen from Fig. 3, performance of the model is limited to a certain level both in time and location predictions. This is due to the simple structure of the model, which is a linear combination of the past sample times and locations.

Another method for comparison is the standard RNN model, which predicts the displacement in time and space using the state vector. The state transition is computed as

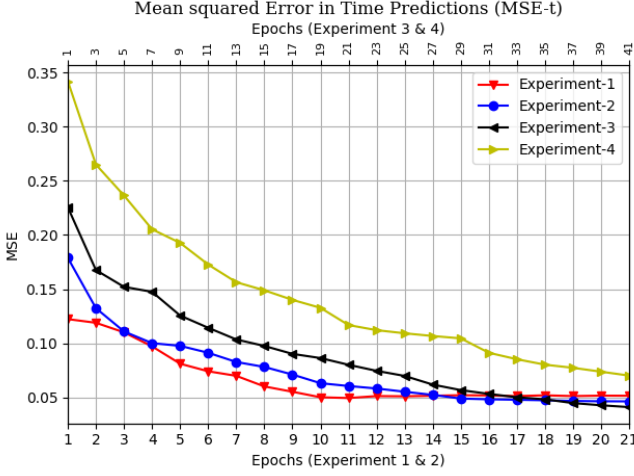
$$\mathbf{h}_i = \tanh(\mathbf{W}_x^T [\Delta t_{i-1}, \Delta x_{i-1}, \Delta y_{i-1}] + \mathbf{W}_h^T \mathbf{h}_{i-1}),$$

where $\tanh = (e^x - e^{-x}) / (e^x + e^{-x})$. We compute the displacements as

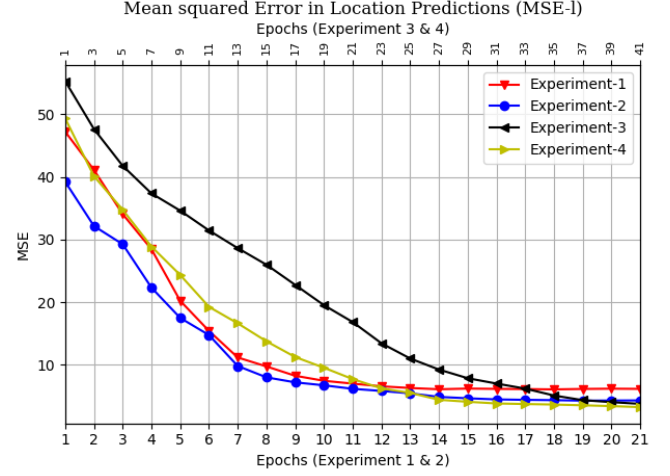
$$\begin{aligned}\Delta t_i &= \mathbf{w}_{t0}^T \mathbf{h}_i, \\ \Delta x_i &= \mathbf{w}_{x0}^T \mathbf{h}_i, \\ \Delta y_i &= \mathbf{w}_{y0}^T \mathbf{h}_i.\end{aligned}$$

For this model, we obtain better results compared to the linear model both in time and location predictions. The reason behind this performance increase is due to the nonlinearity and the inherent state introduced by the RNN transition equations. Instead of using a fixed number of past sample times and locations for prediction, this model computes the predictions using the state vector. As it can be seen from Fig. 3 and Table II, RNN performs significantly better compared to the linear model.

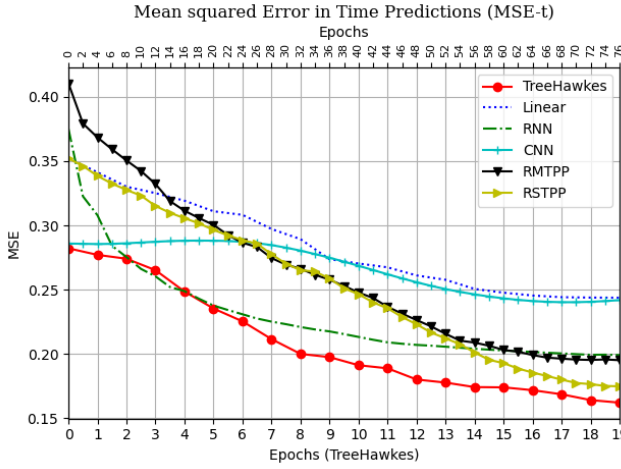
To compare the effect of working directly on the continuous data, we preprocess the spatio-temporal data sequence into a discrete tensor structure. We construct a spatio-temporal tensor with dimensions (T, X, Y) , where T is the total number of temporal bins. X and Y are the total number of spatial bins in both spatial axes. Each temporal bin corresponds to a fixed-length time window. Similarly, each spatial bin in the $X \times Y$ array corresponds to a fixed-area region with identical shapes. Temporal boundaries of our data is between the time of the first event and the last event. We choose the dimension T so that a fixed temporal window between the interval corresponds to 5 days. We select the number of spatial bins in two axes as $X, Y = (30, 30)$. After obtaining the tensor with shape (T, X, Y) , we assign the samples $\{\mathbf{n}_i\}$ into the spatio-temporal



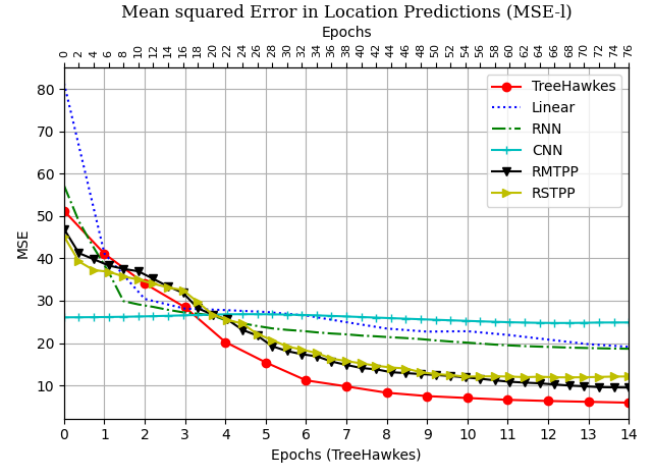
(a) Mean squared error in the temporal predictions of our algorithm with different hyperparameter sets on the simulated data.



(b) Mean squared error in the spatial location predictions of our algorithm with different hyperparameter sets on the simulated data.



(c) Mean squared error in temporal predictions of our algorithm on the real-life earthquake data.



(d) Mean squared error in spatial location predictions of our algorithm on the real-life earthquake data.

Fig. 3: Validation performances obtained on the simulated and real-life data. MSE scores in temporal and spatial axes are recorded at the end of each optimization iteration described in Algorithm 1. Performance of our approach is compared to the standard and baseline approaches in figures (c) and (d) on the real-life earthquake dataset.

bins in the tensor. If an earthquake has occurred in a spatio-temporal bin, it will be labeled as 1 and 0 otherwise. We define the term \mathbf{F}_t as a single spatial frame with shape (X, Y) at temporal bin t . Therefore, we represent the whole data as $\mathcal{F} = \{\mathbf{F}_t\}_{t=1}^T$, which forms the spatio-temporal data.

We use a CNN model, which processes the discrete data structure and predicts the next event time and location. For every time step $t \in \{1, \dots, T\}$, we make a prediction using the most recent 20 frames, i.e. $\{\mathbf{F}_{t-i}\}_{i=1}^{20}$ (corresponds to 100 days). The model applies $30 \times 3 \times 3$ convolutional kernels to the most recent frames and generates a tensor $\{\hat{\mathbf{F}}_{t+i}\}_{i=0}^{29}$ with shape $(30, 30, 30)$. During prediction, this spatio-temporal frame is normalized along all axes and a prediction is computed by computing the center of mass of the spatio-temporal frame. Therefore, next event time and location is predicted by finding the center of mass along three axes as

$$\begin{aligned}\hat{t} &= \sum_{i=0}^{29} c_t^{(t+i)} \sum_{x=1}^X \sum_{y=1}^Y \hat{\mathbf{F}}_{t+i}^{(x,y)}, \\ \hat{x} &= \sum_{i=0}^{29} \sum_{x=1}^X c_x^{(x)} \sum_{y=1}^Y \hat{\mathbf{F}}_{t+i}^{(x,y)}, \\ \hat{y} &= \sum_{i=0}^{29} \sum_{x=1}^X \sum_{y=1}^Y c_y^{(y)} \hat{\mathbf{F}}_{t+i}^{(x,y)},\end{aligned}$$

where $\hat{\mathbf{F}}_{t+i}^{(x,y)}$ corresponds to the spatio-temporal bin at time $t+i$ and at the location x, y in the spatio-temporal tensor. $c_t^{(t+i)}$ is the time corresponding to the $(t+i)$ th temporal bin. Similarly, $c_x^{(x)}$ and $c_y^{(y)}$ are the actual locations corresponding to the x th and y th index in the array.

During the training, we minimize the mean squared error between the generated 30 frames $\{\hat{\mathbf{F}}_{t+i}\}_{i=0}^{29}$ and the ground

truth 30 frames $\{\mathbf{F}_{t+i}\}_{i=0}^{29}$ over the whole training session. We update the model parameters using the ADAM optimizer with respect to the mean squared error between the generated frames and the ground-truth frames. For model evaluation, we pair the predicted times and locations at every step with the ground truth samples that are temporally closest and earlier than the ground-truth sample, i.e. $\hat{t} = \arg \min_t (t_i - \hat{t})^2$ and $\hat{t} \leq t_i$. For each ground-truth sample, we compute the mean squared difference between the actual time and location and the predicted times and locations. Finally, we average the difference scores for all ground-truth samples.

As it can be seen from Fig. 3, CNN performs significantly worse compared to the RNN model and slightly better than the linear model in the temporal predictions. Despite the convolution kernel mechanism in the model, location prediction ability is the worst among all models. This is due to the preprocessing step, which converts the data to a structured format that changes the continuous nature of the data. Since the data consists of irregularly spaced and continuously distributed samples, converting it to a spatio-temporal tensor results in a sparse data. Due to the discretization stage, model predictions become less precise as it can be seen from Fig. 3 and Table II.

Finally, we compare our model with the point process based approaches. First, we test the check-in time prediction model presented in [8] (we refer to as RSTPP). Here, an RNN is used to extract temporal features from the historical check-in times of users. Combining with the user trajectory informations, the intensity is computed as

$$\lambda(t, \mathbf{l} | \Omega(t)) = \exp(\mathbf{w}_h \mathbf{h}_i + w_t(t - t_{i-1}) + w_l \|\mathbf{l} - \mathbf{l}_{i-1}\|^2 + b), \quad (48)$$

where \mathbf{h}_i is the state vector of the RNN model, which has the state transition

$$\mathbf{h}_i = \tanh(\mathbf{W}_x^T \mathbf{x}_{i-1} + \mathbf{W}_h^T \mathbf{h}_{i-1}). \quad (49)$$

Originally, user activity features and past check-in time and locations were included in the vector \mathbf{x}_i . However, we only use the past time and location information. Performance of this approach is significantly better compared to the baseline models, which either expect a discretized data or predict the next time and location of the samples with simple models. On the other hand, this model uses a point process based approach, which directly models the event observations and yields a significantly better performance. However, our model outperforms this approach especially in the location predictions as this model incorporates the location information to the intensity with an additive term, which limits the performance.

Similar to the check-in time prediction, Recurrent Marked Temporal Point Process (RMTTP) approach also estimates the intensity via an RNN [7]. However, in this case, the intensity is defined only for the temporal axis and the location is predicted with markers. Both the intensity and the location markers are computed from the state vector of the RNN model. Similar to the RSTPP model, this approach also outperforms the baseline models and yields a similar performance to the RSTPP model. Again the spatial predictions are limited by the incorporation

and prediction of the spatial location.

We train our model as described in Algorithm 1. We report the difference scores $MSE-t$ and $MSE-l$ on the validation set as shown in Fig. 3. We also report the errors in the test set in Table II.

V. CONCLUDING REMARKS

We introduce a novel spatio-temporal prediction model that predicts the times and locations of the samples using the times and locations of the past samples. Our approach is based on the point processes where we aim to directly model the samples via a probabilistic model. Our formulations are based on the Hawkes process, but can be readily extended to other point process models depending on the application. We also incorporate the spatial connections between the past sample locations and the intensity function via a kernel mechanism. Furthermore, we also partition the spatial region into subregions via an adaptive decision tree. Therefore, we optimize our point process parameters jointly with the sub-region boundaries using a likelihood based objective function and the stochastic gradient descent method. Thanks to self-exciting and nonstationary intensity formulation of our point process and the adaptive partitioning mechanism, we are able to represent highly sparse and nonstationary data. Finally, we demonstrate significant performance improvements of our model with an extensive set of experiments where we compare our model with the baseline and standard approaches on a real-life earthquake dataset.

REFERENCES

- [1] M. Xu, Y. Yang, M. Han, T. Qiu, and H. Lin, "Spatio-temporal interpolated echo state network for meteorological series prediction," *IEEE Transactions on Neural Networks and Learning Systems*, vol. 30, no. 6, pp. 1621–1634, 2019.
- [2] V. Roberto and C. Chiaruttini, "Seismic signal understanding: a knowledge-based recognition system," *IEEE Transactions on Signal Processing*, vol. 40, no. 7, pp. 1787–1806, 1992.
- [3] H. Quan, A. Khosravi, D. Yang, and D. Srinivasan, "A survey of computational intelligence techniques for wind power uncertainty quantification in smart grids," *IEEE Transactions on Neural Networks and Learning Systems*, pp. 1–18, 2019.
- [4] B. Wang, P. Yin, A. L. Bertozzi, P. J. Brantingham, S. J. Osher, and J. Xin, "Deep learning for real-time crime forecasting and its ternarization," *Chinese Annals of Mathematics, Series B*, vol. 40, no. 6, pp. 949–966, 2019.
- [5] W. Zhang, X. Lai, and J. Wang, "Social link inference via multiview matching network from spatiotemporal trajectories," *IEEE Transactions on Neural Networks and Learning Systems*, pp. 1–12, 2020.
- [6] C. Alippi, M. Roveri, and F. Trovò, "A self-building and cluster-based cognitive fault diagnosis system for sensor networks," *IEEE Transactions on Neural Networks and Learning Systems*, vol. 25, no. 6, pp. 1021–1032, 2014.
- [7] N. Du, H. Dai, R. Trivedi, U. Upadhyay, M. Gomez-Rodriguez, and L. Song, "Recurrent marked temporal point processes: Embedding event history to vector," in *Proceedings of the 22nd ACM SIGKDD International Conference on Knowledge Discovery and Data Mining*, 2016, pp. 1555–1564.
- [8] G. Yang, Y. Cai, and C. K. Reddy, "Recurrent spatio-temporal point process for check-in time prediction," in *Proceedings of the 27th ACM International Conference on Information and Knowledge Management*, 2018, pp. 2203–2211.
- [9] J. Wang, J. Tang, Z. Xu, Y. Wang, G. Xue, X. Zhang, and D. Yang, "Spatiotemporal modeling and prediction in cellular networks: A big data enabled deep learning approach," in *IEEE INFOCOM 2017-IEEE Conference on Computer Communications*. IEEE, 2017, pp. 1–9.
- [10] J. L. Elman, "Finding structure in time," *Cognitive Science*, vol. 14, no. 2, pp. 179–211, 1990.
- [11] S. Hochreiter and J. Schmidhuber, "Long short-term memory," *Neural Computation*, vol. 9, no. 8, pp. 1735–1780, 1997.

- [12] L. Duan, T. Hu, E. Cheng, J. Zhu, and C. Gao, "Deep convolutional neural networks for spatiotemporal crime prediction," in *Proceedings of the International Conference on Information and Knowledge Engineering (IKE)*. The Steering Committee of The World Congress in Computer Science, Computer . . . , 2017, pp. 61–67.
- [13] H. Yu, Z. Wu, S. Wang, Y. Wang, and X. Ma, "Spatiotemporal recurrent convolutional networks for traffic prediction in transportation networks," *Sensors*, vol. 17, no. 7, p. 1501, 2017.
- [14] Z. Gao, X. Wang, Y. Yang, C. Mu, Q. Cai, W. Dang, and S. Zuo, "Eeg-based spatio-temporal convolutional neural network for driver fatigue evaluation," *IEEE Transactions on Neural Networks and Learning Systems*, vol. 30, no. 9, pp. 2755–2763, 2019.
- [15] H. Mei and J. M. Eisner, "The neural hawkes process: A neurally self-modulating multivariate point process," in *Advances in Neural Information Processing Systems*, 2017, pp. 6754–6764.
- [16] B. Wang, D. Zhang, D. Zhang, P. J. Brantingham, and A. L. Bertozzi, "Deep learning for real time crime forecasting," *arXiv preprint arXiv:1707.03340*, 2017.
- [17] D. R. Cox and V. Isham, *Point processes*. CRC Press, 1980, vol. 12.
- [18] D. J. Daley and D. Vere-Jones, *An introduction to the theory of point processes: volume II: general theory and structure*. Springer Science & Business Media, 2007.
- [19] H. Kanamori, "Earthquake prediction: An overview," 2003.
- [20] A. Krizhevsky, I. Sutskever, and G. E. Hinton, "Imagenet classification with deep convolutional neural networks," in *Advances in Neural Information Processing Systems*, 2012, pp. 1097–1105.
- [21] Y. Wang, B. Xie, N. Du, and L. Song, "Isotonic hawkes processes," in *International Conference on Machine Learning*, 2016, pp. 2226–2234.
- [22] B. Wang, X. Luo, F. Zhang, B. Yuan, A. L. Bertozzi, and P. J. Brantingham, "Graph-based deep modeling and real time forecasting of sparse spatio-temporal data," *arXiv preprint arXiv:1804.00684*, 2018.
- [23] G. Ö. Mohler, M. B. Short, P. J. Brantingham, F. P. Schoenberg, and G. E. Tita, "Self-exciting point process modeling of crime," *Journal of the American Statistical Association*, vol. 106, no. 493, pp. 100–108, 2011.
- [24] B. Cseke, A. Zammit-Mangion, T. Heskes, and G. Sanguinetti, "Sparse approximate inference for spatio-temporal point process models," *Journal of the American Statistical Association*, vol. 111, no. 516, pp. 1746–1763, 2016.
- [25] M. Adepeju, G. Rosser, and T. Cheng, "Novel evaluation metrics for sparse spatio-temporal point process hotspot predictions-a crime case study," *International Journal of Geographical Information Science*, vol. 30, no. 11, pp. 2133–2154, 2016.
- [26] M. Jacobsen, *Point process theory and applications: marked point and piecewise deterministic processes*. Springer Science & Business Media, 2006.
- [27] A. Alahi, K. Goel, V. Ramanathan, A. Robicquet, L. Fei-Fei, and S. Savarese, "Social lstm: Human trajectory prediction in crowded spaces," in *Proceedings Of The IEEE Conference On Computer Vision And Pattern Recognition*, 2016, pp. 961–971.
- [28] E. Lewis and G. Mohler, "A nonparametric em algorithm for multiscale hawkes processes," *Journal of Nonparametric Statistics*, vol. 1, no. 1, pp. 1–20, 2011.
- [29] V. Isham and M. Westcott, "A self-correcting point process," *Stochastic Processes And Their Applications*, vol. 8, no. 3, pp. 335–347, 1979.
- [30] T. K. Ho, "Random decision forests," in *Proceedings of 3rd international conference on document analysis and recognition*, vol. 1. IEEE, 1995, pp. 278–282.
- [31] J. Ali, R. Khan, N. Ahmad, and I. Maqsood, "Random forests and decision trees," *International Journal of Computer Science Issues (IJCSI)*, vol. 9, no. 5, p. 272, 2012.
- [32] B. C. Csáji *et al.*, "Approximation with artificial neural networks," *Faculty of Sciences, Eötvös Loránd University, Hungary*, vol. 24, no. 48, p. 7, 2001.
- [33] F. M. Willems, Y. M. Shtarkov, and T. J. Tjalkens, "The context-tree weighting method: basic properties," *IEEE Transactions on Information Theory*, vol. 41, no. 3, pp. 653–664, 1995.
- [34] B. P. Flannery, W. H. Press, S. A. Teukolsky, and W. Vetterling, "Numerical recipes in c," *Press Syndicate of the University of Cambridge, New York*, vol. 24, p. 78, 1992.
- [35] R. E. Caflisch, "Monte carlo and quasi-monte carlo methods," *Acta Numerica*, vol. 7, pp. 1–49, 1998.
- [36] L. Bottou, "Large-scale machine learning with stochastic gradient descent," in *Proceedings of COMPSTAT'2010*. Springer, 2010, pp. 177–186.
- [37] D. P. Kingma and J. Ba, "Adam: A method for stochastic optimization," *arXiv preprint arXiv:1412.6980*, 2014.
- [38] Y. Ogata, "On lewis' simulation method for point processes," *IEEE Transactions on Information Theory*, vol. 27, no. 1, pp. 23–31, 1981.
- [39] N. E. I. Center, "Significant earthquakes," <https://www.usgs.gov/natural-hazards/earthquake-hazards/earthquakes>, 2020.
- [40] J. D. Hamilton, *Time series analysis*. Princeton New Jersey, 1994, vol. 2.